Investigation of fiber volume fraction as key parameter in cryogenic hydrogen tank development

Appels, Jonas P.; Sämann, Philipp; Naumann, Jonas; Brauer, Christoph; Stefaniak, Daniel; Atli-Veltin, Bilim; Dransfeld, Clemens

DOI
10.33599/nasampe/s.25.0109

Publication date
2025

Document Version
Final published version

Published in
SAMPE 2025 Conference and Exhibition

INVESTIGATION OF FIBER VOLUME FRACTION AS KEY PARAMETER IN CRYOGENIC HYDROGEN TANK DEVELOPMENT

Jonas P. Appels[1,2], Philipp Sämann[1], Jonas Naumann[1], Christoph Brauer[1], Daniel Stefaniak[1,2], Bilim Atli-Veltin[2], Clemens Dransfeld[2]
1 - Institute of Lightweight Systems, German Aerospace Center (DLR), Stade, Germany
2 - Faculty of Aerospace Engineering, Delft University of Technology, Netherlands

ABSTRACT

In developing Type V hydrogen tanks for energy storage in commercial airliners, the key design criterion is maintaining leak-tightness under cryogenic conditions. A concern is that anomalies in the laminate could cause microcracks, potentially compromising leak-tightness. This study investigates how resin flow, caused by mandrel expansion during curing, creates a gradient in the local fiber volume fraction (FVF) along the laminate thickness. An experimental study was performed comparing two resin systems, Hexcel 6376 and Teijin Q183. Cylindrical specimens were manufactured incorporating piezoresistive sensors to measure contact pressure at the mandrel-laminate interface during the autoclave cycle, serving as an indicator of resin flow and FVF variation. Micrographs of the specimen were taken, and a machine learning-based segmentation model was used to detect fibers and resin in the images, enabling calculation of the local FVF. The results show distinct through-the-thickness gradients in FVF for both laminates with a spread of 11.6 %pt. for Hexcel 6376 and 4.5 %pt. for Teijin Q183. These observations could be correlated to the processing characteristics of the two systems and therefore provide valuable insights for developing strategies to minimize FVF gradients in the design of carbon fiber-reinforced polymer (CFRP) tanks for liquid hydrogen.

Keywords: Cryogenic Hydrogen Tank; Resin Flow; Fiber Volume Fraction

Corresponding author: Jonas P. Appels (jonas.appels@dlr.de)

1. INTRODUCTION

Hydrogen is emerging as a promising solution for decarbonizing the aviation sector due to its potential for zero-emission operation and advancements in supporting technologies [1]. Unlike conventional aviation fuels, hydrogen combustion or utilization in turbines and fuel cells primarily produces water vapor, eliminating CO_2 emissions. However, the successful transition to hydrogen-powered aviation necessitates significant technological innovations, particularly in the development of lightweight and efficient cryogenic storage systems [2].

Integrating a hydrogen tank into an aircraft involves complex structures, leading to an overall increase in weight. Various aircraft concepts indicate that the operational empty weight (OEW) could increase by approximately 23 % due to the structural requirements of liquid hydrogen

SAMPE Conference Proceedings. Indianapolis, IN, May 19-22, 2025. Society for the Advancement of Material and Process Engineering – North America.

DOI: https://doi.org/10.33599/nasampe/s.25.0109

(LH_2) tanks [3]. This substantial weight increase underscores the necessity of developing innovative lightweight solutions for cryogenic hydrogen storage.

Cryogenic pressure vessels can generally be categorized into five types, ranging from Type I to Type V [4]. Among these, Type V tanks are constructed entirely from continuous fiber-reinforced composites without an internal liner. This design approach requires the composite material to fulfill dual roles: serving as both the primary load-bearing structure as well as ensuring leak tightness. Despite those challenges, Type V tanks offer several advantages, including reduced weight, simplified manufacturing, potentially lower certification complexity by eliminating the liner, and enhanced fatigue resistance due to the absence of a strain compatibility at the interface to the liner [5]. However, when subjected to cryogenic conditions, these tanks are prone to microcracking, which may compromise their leak-tightness [6].

One potential factor contributing to microcrack formation is the presence of inhomogeneities in the laminate, which may exacerbate crack initiation and propagation [7]. A specific inhomogeneity observed in CFRP laminates is the variation in the local fiber volume fraction (FVF) along the thickness of the laminate. It is hypothesized that this variation arises due to the thermal expansion of the mandrel during the autoclave curing cycle. While metals such as aluminum and steel exhibit a positive coefficient of thermal expansion (CTE), carbon fibers possess a near-zero or even negative CTE in fiber direction [8].When the tapes are wound circumferentially around a mandrel, as seen in Figure 1, the mandrel's expansion exerts tensile forces on the fibers. This interaction generates contact pressure at the interface between the laminate and the mandrel. During a short viscosity drop at elevated temperatures, the resin - being more fluid - tends to flow outward, while the tensioned fibers move inward to relieve stress. This process is believed to induce an FVF gradient through the laminate thickness. A too high FVF can be detrimental to transverse tensile strength [9]. Material suppliers therefore specify FVF values with high precision to ensure optimal mechanical properties [10]. Understanding the origins of this gradient is therefore crucial for controlling laminate quality.

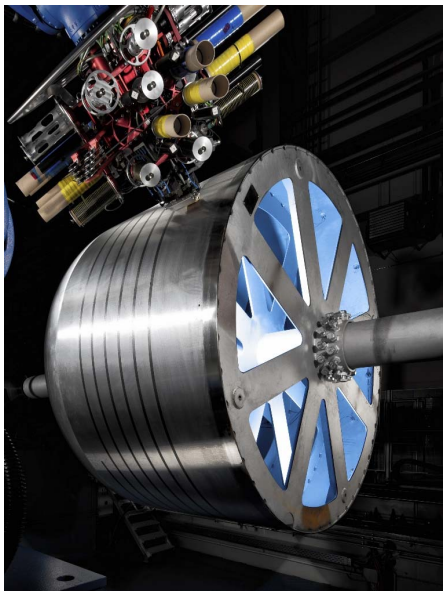

Figure 1. Tank demonstrator with mandrel (⌀ 3 m) on rotational axis and AFP end-effector. Developed for the DLR HyStor project [11].

The primary objective of this study is to investigate how the thermal expansion of the mandrel induces the resin flow and contributes to the formation of an FVF gradient across the thickness of CFRP laminates. The study specifically aims to elucidate the physical and rheological mechanisms underlying this phenomenon. Investigating the potential impact of the FVF gradient on microcrack behavior, however, is beyond the scope of this study.

This report is intended for researchers, engineers and stakeholders in aerospace materials and manufacturing industries involved in the development and manufacturing of tank structures made from CFRP, especially for use as cryogenic hydrogen tanks in aviation. The content assumes a basic understanding of composite materials, manufacturing processes, and hydrogen technology but does not require prior expertise in cryogenic storage systems.

The experimental study compared two different materials on the through-thickness FVF gradient of tank structures. Section 2 presents the experimental procedure which includes the specimen manufacturing and the specimen analysis. Section 3 outlines the results from the micrographs with heatmaps and the contact pressure graphs. Section 4 concludes the paper with the most important take-aways of this experimental study.

2. EXPERIMENTATION

2.1 Materials and Manufacturing

To systematically investigate the phenomenon of resin flow, the study utilized tubular specimens with a diameter of 350 mm. Figure 2 presents such a cured specimen positioned in front of the mandrel on which it was manufactured. This geometry was selected due to its optimal balance between cost efficiency, high knowledge gain and fast manufacturing.

Figure 2. Tubular specimen (⌀ 350 mm) in front of aluminum mandrel.

For this experimental study the resin systems were chosen to cover two different types of thermoset resin systems. One system shall be a conventional system without tougheners while the other shall be a fast-cure system with tougheners. Finally the choice was made for Hexcel 6376 and Teijin Q183. Hexcel 6376 is a conventional, untoughened, and well-established resin system, whereas Teijin Q183 is a toughened, rapid-cure system. Due to the material availability at the time of this study it was not possible to choose the same fibers and areal weights for both

materials. A summary of the key material properties is provided in Table 1. The specimens were cured in the autoclave according to the procedure recommended by the respective material supplier.

Table 1. Material specifications as provided by the material suppliers [12] [13].

		TEIJIN	HEXCEL
Matrix	Name	Q183	HexPly 6376
	Curing temp.	160 °C	175 °C
	Holding phase	20 min	120 min
Fiber	Name	IMS65	Tenax HTS
	Nr. of filaments	24k	12k
	Tensile modulus	290 GPa	240 GPa
	FVF	65 % (supplier data)	58 % (lab measurement)
	Areal weight	145 gsm	194 gsm

Automated Fiber Placement (AFP) was considered as the most promising manufacturing technology for Type V hydrogen tanks [4]. However, instead of employing an AFP end-effector for this study, a custom manufacturing rig was developed to enable a simpler, more cost-effective, and faster specimen fabrication, eliminating reliance on complex machinery. Figure 3 provides a schematic of this rig, while Figure 4 shows its final implementation.

On this rig, the specimens were fabricated by winding prepreg tape around the mandrel in 12 circumferential revolutions. The two rollers positioned beneath the mandrel function as a compaction mechanism, mimicking the compaction roller of an AFP end-effector. The applied compaction force was adjusted by placing weights on a cart inside the mandrel and was set to 2.5 N/mm (compaction force per tape width) per roller. An electric motor controlled the placement speed, while a three-roller tensioning system on the left regulated fiber tension during placement. The weights in the tensioning system were chosen to yield a tension of 0.356 N/mm (tension per tape width) which is a common value for AFP end-effectors [14].

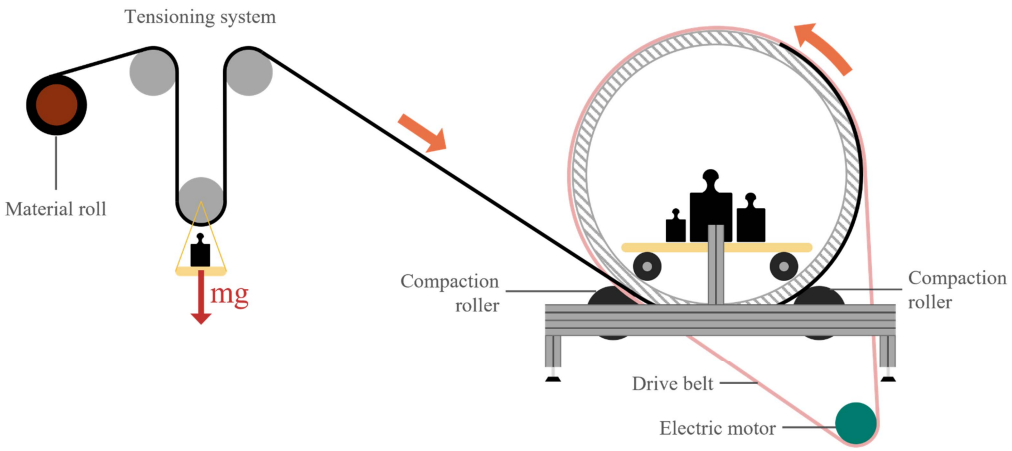

Figure 3. Schematic of manufacturing rig.

Figure 4. Implementation of manufacturing rig.

2.2 Specimen Analysis

2.2.1 Material Characterization

To analyze the flow and curing behavior of the two resin systems used in this study, two material characterization methods were performed: a rheology study and differential scanning calorimetry (DSC). Both tests were conducted on the full composite system, including both resin and fibers, as pure resin samples from the prepreg were unavailable.

The rheology study was performed in an Anton Paar MCR702 rheometer in strain-controlled mode using a parallel plate setup, following a temperature cycle equivalent to the recommended autoclave curing process for each resin system. DSC analysis was conducted using the Mettler Toledo TOPEM method [15], which superimposes the temperature ramp with random low-amplitude temperature pulses of varying duration. This approach enabled the separation of total heat flow into reversing and non-reversing heat flow components of which the latter was used to determine the degree of cure. The baseline temperature cycle also followed the recommended curing cycle.

2.2.2 Contact Pressure Sensor

According to the hypothesis, resin flow in the thickness direction correlates with fiber tension and the contact pressure at the interface between the mandrel and the laminate, which is induced by the thermal expansion of the tool. This contact pressure can be directly measured using a thin piezoresistive sensor placed between the mandrel and the laminate, as illustrated in Figure 5. Both specimens in this study were equipped with such a sensor, which continuously recorded data throughout the entire autoclave curing cycle. The FlexiForce HT201 [16] by Tekscan was selected for this application. It is a force sensor specifically designed for high-temperature environments, with an operating range of up to 200 °C. With a thickness of just 0.203 mm, the sensor is relatively thin compared to the 350 mm diameter of the specimens and therefore has a negligible impact on the specimen. The sensor was integrated during the winding process, with its sensing area positioned right underneath the laminate and its contact pins extending outward for easy accessibility. The sensor's smooth surface facilitated leak-tight incorporation into the vacuum bagging process.

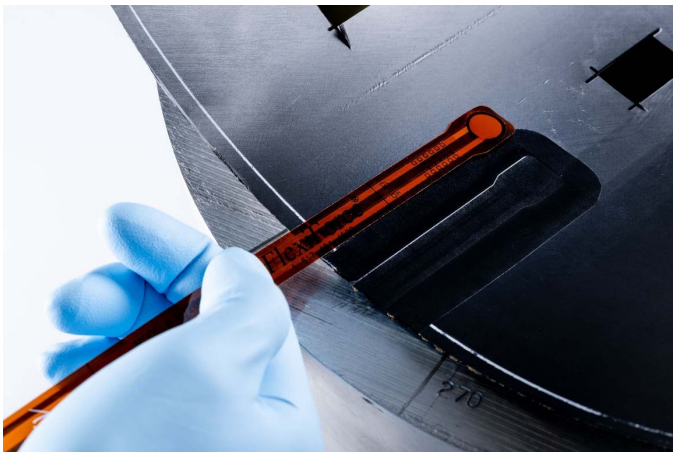

Figure 5. Tekscan FlexiForce HT201 contact pressure sensor.

2.2.3 Temperature Measurement

To track the thermal expansion of the tool and curing progression of the prepreg material, it was essential to monitor the temperature at the interface between the mandrel and the laminate. However, to avoid disrupting the specimen with thick thermocouples, a traveler specimen of the same material and layup was added to each mandrel. This traveler specimen was placed on top a Type J thermocouple fixed on the mandrel.

2.2.4 Micrographs & Optical Microscopy

The specimen analysis proceeded with an investigation of the laminate cross-section using optical microscopy. To achieve this, micrographs were prepared from the specimens. The extracted samples were oriented with the fibers perpendicular to the observation surface, then embedded in potting resin for stabilization and subjected to a polishing process. As shown in Figure *6*, the micrographs were captured using a Keyence VHX-5000 digital microscope at 500× magnification. A 2D stitching procedure was applied, incorporating automatic depth composition to capture a larger section of the laminate.

Figure 6. Embedded micrograph underneath optical microscope.

3. RESULTS AND DISCUSSION

3.1 Micrographs and Heatmaps

Figure 7 presents the micrograph of the Hexcel 6376 specimen, while Figure 8 shows the micrograph of the Teijin Q183 specimen. Already through visual inspection, a noticeable difference in FVF distribution can be observed in the case of Hexcel 6376. The FVF appears to be higher on the mandrel-facing side, gradually decreasing further away from it. However, for Teijin Q183, this trend is less apparent in the micrographs, suggesting a potentially different resin flow behavior during the curing process.

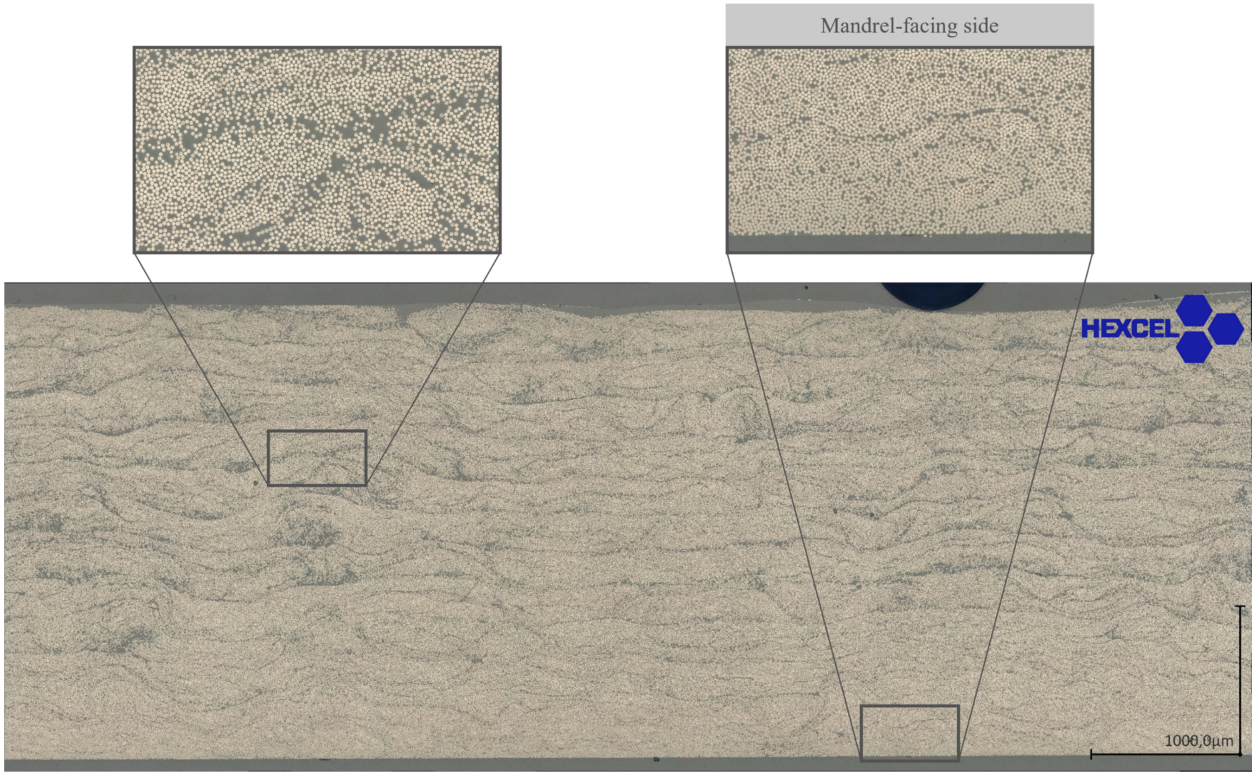

Figure 7. Micrograph image of Hexcel 6376.

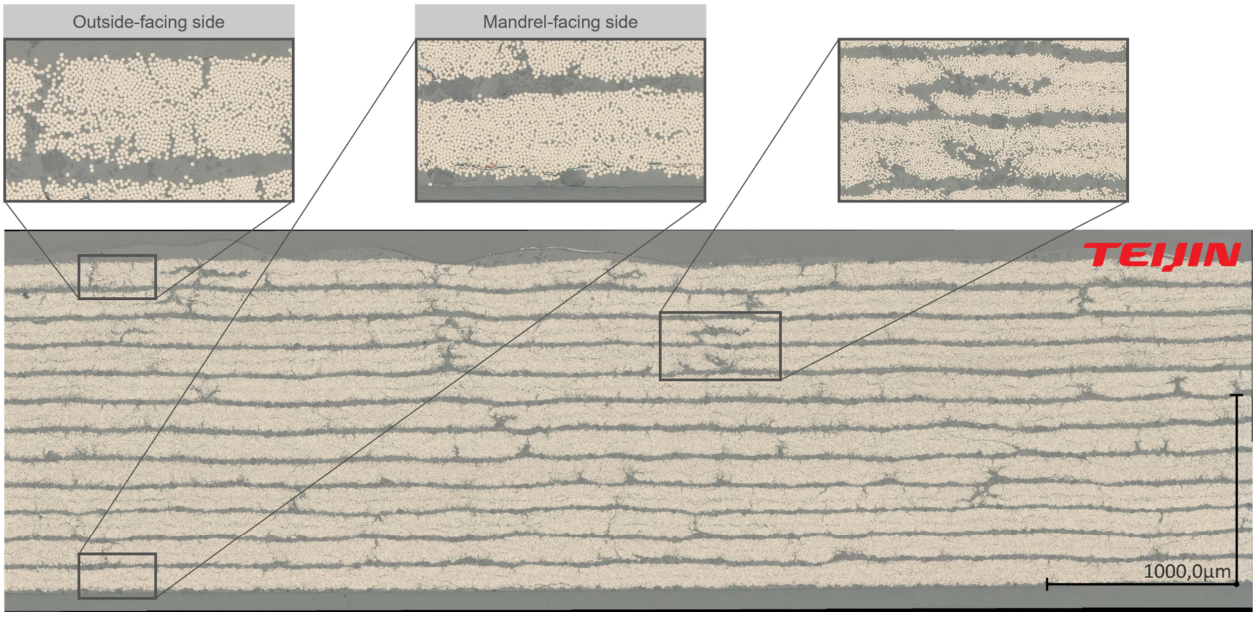

Figure 8. Micrograph image of Teijin Q183.

3.1.1 Semantic Segmentation and FVF Heatmaps

To analyze the resin distribution and FVF quantitatively and automatically, a machine learning-based computer vision model, described in detail in [17], was applied to classify each pixel in the digital micrograph. The used semantic segmentation model is based on a modified U-Net architecture [18] and was trained on more than 3,000 small image patches from seven different CFRP specimens. It assigns each pixel to one of the following classes: 0°, 45°, and 90° fibers, matrix, crack, or others. For this study, only the pixels classified as 0° fiber or matrix were relevant.

The resulting segmentation masks were used to compute the local FVF at every tenth pixel position in both dimensions by evaluating the surrounding pixels within a square 301×301 pixel neighborhood. The size was chosen to be in the range of the ply thickness of Teijin Q183. The local FVF was determined as the ratio of 0° fiber pixels to the total pixels within the neighborhood. Pixels classified as any class other than 0° fiber and matrix are omitted completely for this calculation. The resulting FVF distribution was visualized as a semi-transparent heatmap overlay on the micrograph, as illustrated in Figure 9 and Figure 10.

Since the model does not distinguish between matrix and embedding material, a limitation of this methodology is evident at the upper and lower boundaries of the CFRP sample, where the FVF appears to decrease sharply. This artifact arises, because, near the sample's boundary, the defined neighborhood extends beyond the physical sample, incorporating regions of embedding material into the calculation and artificially lowering the FVF. While this issue is confined to the sample edges and does not affect the central regions of the micrograph, it represents a methodological drawback that will be addressed in future refinements.

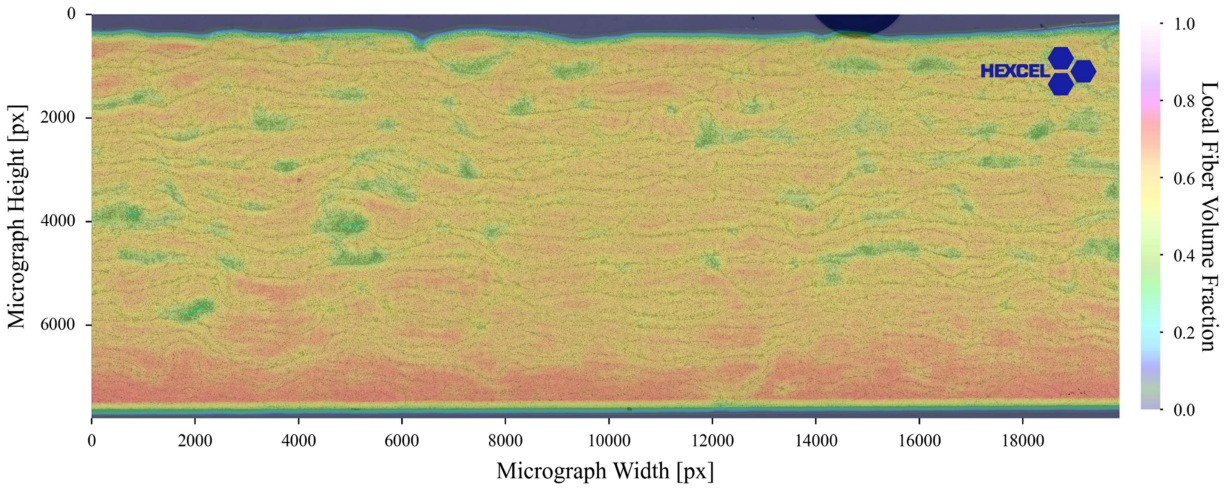

Figure 9. Heatmap of Hexcel 6376.

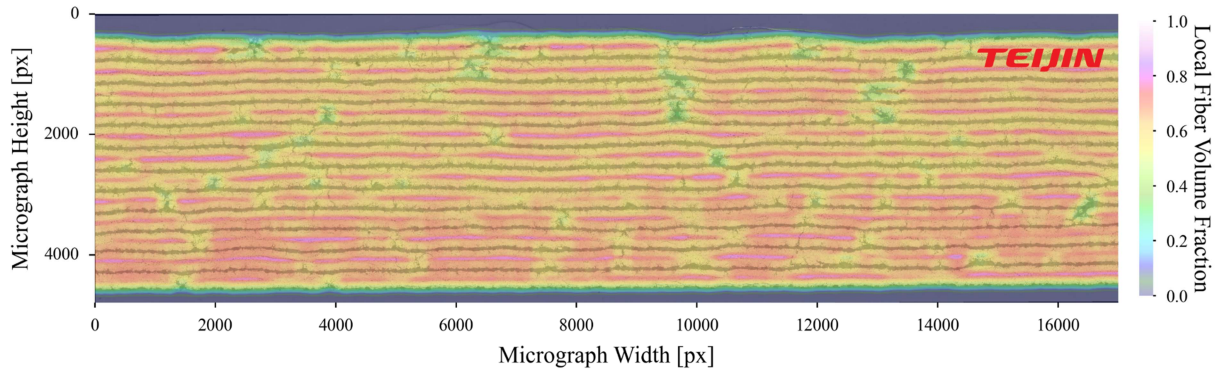

Figure 10. Heatmap of Teijin Q183.

3.1.2 FVF Spread

Figure 11 shows the average through-thickness distribution of the local FVF, highlighting trends across the laminate thickness. Both specimens exhibit 12 peaks, corresponding to the 12 plies wound onto the mandrel. On this scale, intra-ply characteristics, such as the FVF distribution within a single ply, can be observed. However, the resin flow effect investigated in this study occurs at the overall laminate level and is captured by calculating a moving average.

Based on the moving average, Hexcel 6376 shows an FVF range from 56.0 % to 67.6 %, while Teijin Q183 ranges from 62.8 % to 67.3 %. Hexcel 6376 exhibits a much greater variation of 11.6 %pt. compared to 4.5 %pt. for Teijin Q183. This indicates that resin flow occurred in both materials but was significantly more pronounced in Hexcel 6376.

Both specimens show their maximum FVF on the bottom side facing the mandrel, followed by a steep decrease, reaching a minimum after approximately two-thirds of the specimen height. In the upper third, the FVF increases again, likely due to the compression effect of the vacuum foil.

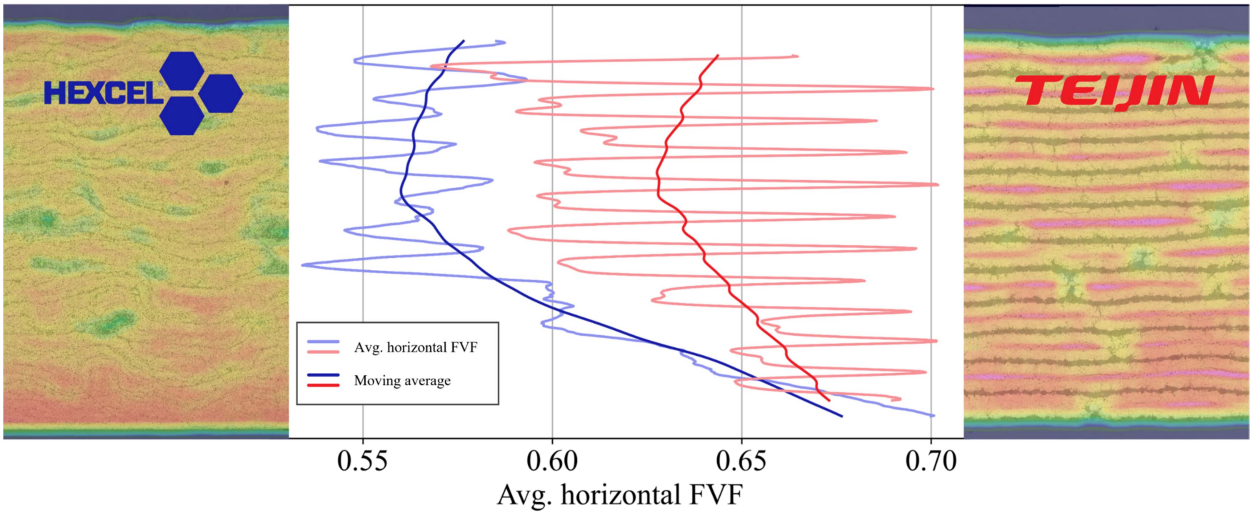

Figure 11. The average FVF for each horizontal line of pixels is plotted, along with its moving average, which is calculated using the arithmetic mean of a specified set of vertical data points.

3.2 Pressure and Temperature Graphs

During the autoclave curing cycle, the mandrel temperature (measured underneath the traveler specimen) and the contact pressure were continuously recorded, and the data was plotted against time. This plot is further enhanced by incorporating viscosity from rheology measurements and the degree of cure determined from the DSC analyses. Both viscosity and degree of cure were measured using a temperature profile matching the autoclave cycle, though minor corrections were applied to account for the mandrel's thermal inertia and the resulting delayed temperature increase. The combined plots are presented in Figure 12 for Hexcel 6376 and

Figure *14* for Teijin Q183.

Prior to implementation, the contact pressure sensors were calibrated using a known force applied to the sensing area. However, the actual loading condition underneath the laminate differs slightly, as the force distribution is more spread out, distorting the absolute values of the pressure reading. Consequently, the y-axis in the plots displays force rather than pressure. Despite this limitation, the qualitative interpretation of the results remains unaffected.

Similarly, since the rheology measurements were conducted on prepreg plies, thus with fibers included, the absolute viscosity values are shifted compared to pure resin, limiting the results to qualitative conclusions.

3.2.1 Hexcel 6376

The pressure graph in Figure 12 can be segmented into different phases, each relating to the thermal expansion of the mandrel and the resin flow. The phases are described in detail below.

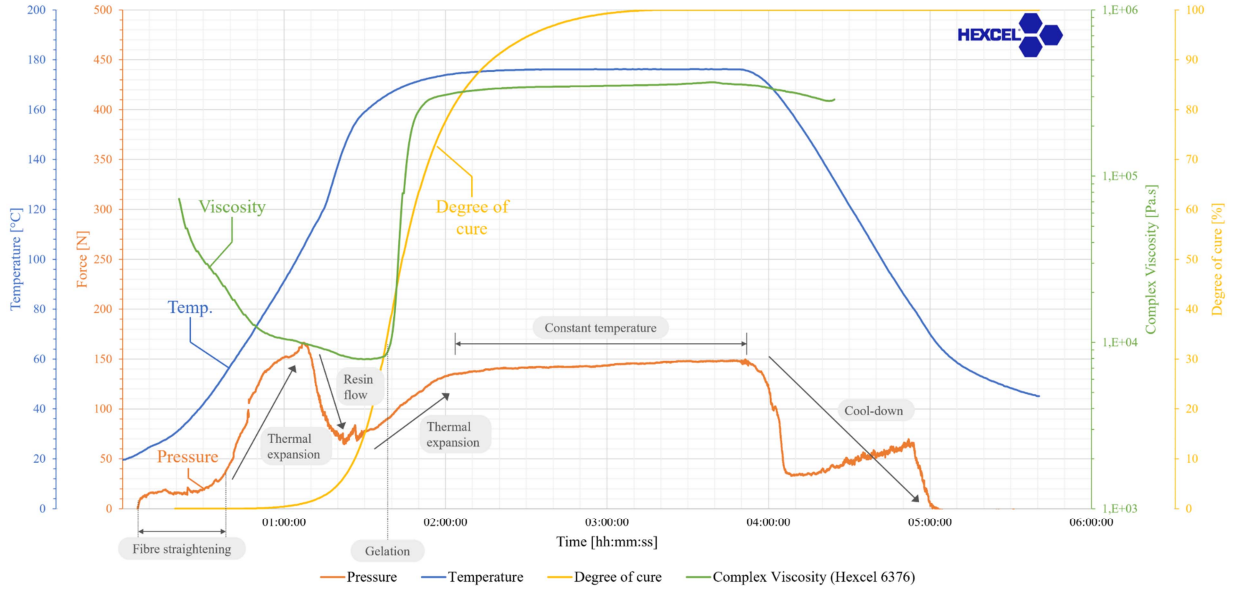

Figure 12. Temperature and pressure graph of Hexcel 6376.

3.2.1.1 Fiber Straightening and Thermal Expansion

At t = 0, the graph begins with the uncured material. As the autoclave temperature increases, the mandrel also heated up, causing thermal expansion and a corresponding increase in mandrel diameter. The fibers wrapped around the mandrel had a coefficient of thermal expansion slightly below zero, resisting the mandrel's expansion and generating pressure at the laminate-mandrel interface. This pressure was recorded by the sensor. While an increase in pressure was expected with rising temperature, the pressure remained relatively constant between 00:07:00 and 00:34:00. This plateau can be attributed to a process referred to as fiber straightening, where the tortuosity, undulations, and manufacturing imperfections of the fibers were gradually flattened. The thermal expansion first had to overcome this initial clearance or free play within the system before the fibers became fully tensioned, allowing a built up of compaction pressure due to fiber hoop stress.

3.2.1.2 Resin Flow

As temperature increases, viscosity decreases, which, according to Darcy's equation [19], leads to an increased resin flow rate. This behavior is also observed in this study. Once the resin viscosity is sufficiently low to overcome viscous drag, it becomes mobile, allowing the fibers to move through the resin closer to the mandrel to release part of the tension. This occurs because the circumference near the mandrel is smaller, reducing fiber elongation and tension. This inward fiber movement generates opposing pressures attributed to fiber compaction and viscous drag respectively, that push the resin outward, effectively creating an exchange where fibers move inward while resin is displaced outward. This phenomenon is illustrated in Figure 13.

Over time, resin flow slows for two reasons. First, as more fibers move closer to the mandrel, they begin making direct contact with adjacent fibers, leaving no additional space for further compression or excess resin displacement. The micrograph of Hexcel 6376 (Figure 7) confirms

this, showing that fibers in the lower section are mostly in direct contact with each other, whereas fibers further away remain surrounded by resin. Second, as curing progresses, resin gelation occurs, causing a rapid increase in viscosity that "locks" the fibers in place hence prohibiting further resin percolation flow. The onset of gelation closely aligns with the steep increase in the degree of cure, demonstrating consistency between the rheology study and the DSC measurements. This correlation is expected, as gelation results from crosslink formation during curing, which restricts molecular mobility.

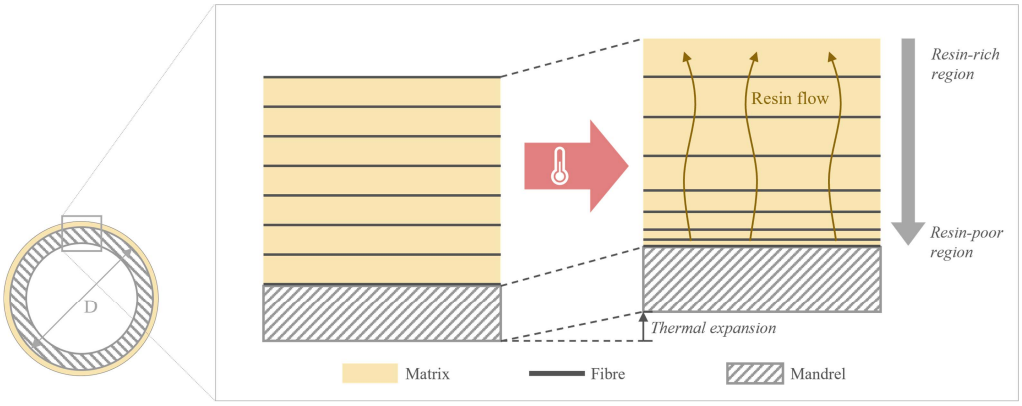

Figure 13. Schematic of resin flow phenomenon.

3.2.1.3 Thermal Expansion

Once resin flow ceases, the fibers can no longer release tension through this mechanism. However, as the mandrel temperature continues to rise, its diameter increases further, leading to a second pressure increase.

3.2.1.4 Constant Temperature

When the temperature reaches a plateau and stabilizes, thermal expansion halts, resulting in a constant pressure level.

3.2.1.5 Cool-down Phase

Following the temperature plateau, the mandrel and laminate begin to cool. As this process is the reverse of thermal expansion, the mandrel contracts, causing a corresponding decrease in pressure.

3.2.2 Comparison with Teijin Q183

Compared to Hexcel 6376, the pressure drop due to resin flow is significantly less pronounced in Teijin Q183 specimens as seen in Figure 14. Instead of a distinct drop, only a temporary change in slope is observed, while the pressure continues to increase monotonically. When comparing the pressure curve with the viscosity curve, it becomes clear that this temporary slope change coincides with the minimum viscosity, indicating a phase of resin flow. However, the magnitude is lower and is largely superimposed by the pressure increase resulting from thermal expansion. This observation aligns with the FVF distribution in the heatmaps, where Teijin Q183 exhibits a significantly lower FVF spread compared to Hexcel 6376.

A comparison of the minimum viscosity values from the respective material data sheets [12] [13] further supports this finding. Teijin Q183 has about the double minimum viscosity, but occurring at a lower temperature (8.6 Pa·s at 100 °C) compared to Hexcel 6376 (3.5 Pa·s at 150 °C). Since viscosity is inversely proportional to resin flow rate according to Darcy's equation, a higher viscosity results in reduced resin flow. Additionally, as Teijin Q183 reaches its minimum viscosity at a lower temperature, the mandrel reaches less thermal expansion, leading to lower fiber tension. This ultimately reduces the pressure driving resin flow, further contributing to the lower observed resin flow rate. These findings highlight the significant influence of the resin system on the FVF gradient.

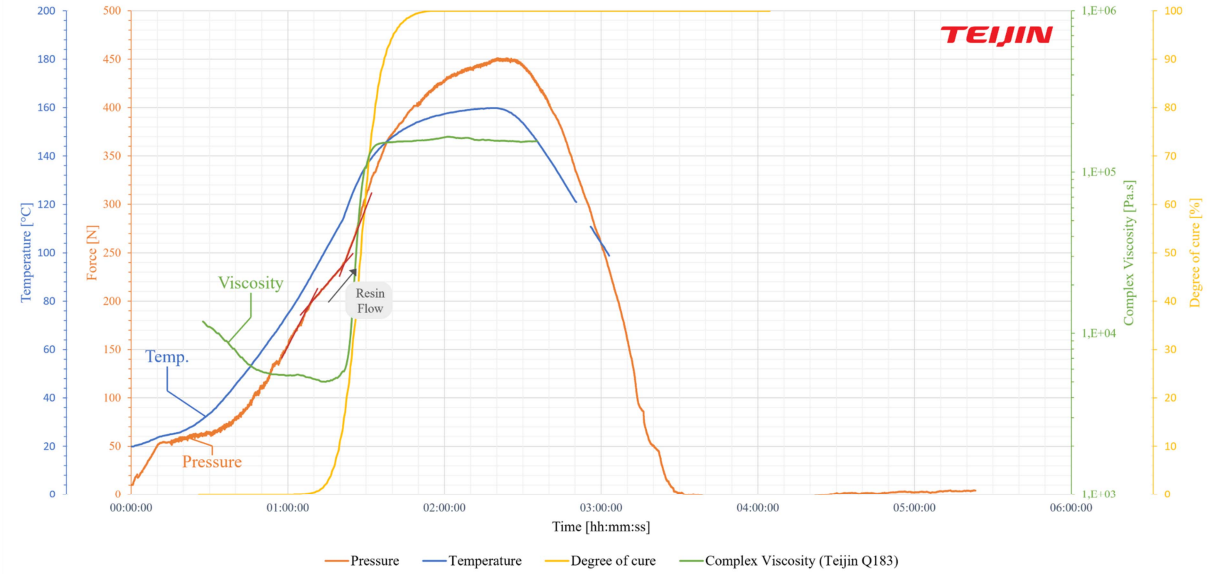

Figure 14. Temperature and pressure graph for Teijin Q183.

3.3 Failure Mechanisms

The results indicate significant local maxima in FVF especially for Hexcel 6376, which may influence the failure mechanisms of the laminate. Since the longitudinal properties of a UD composite material are primarily governed by the fibers, an increase in FVF leads to a higher longitudinal tensile strength. However, the transverse tensile strength decreases with higher FVF, as the applied loads are distributed over a reduced matrix area, resulting in premature failure at the fiber-matrix interface [9]. This effect is particularly pronounced in the region near the mandrel, where fibers are densely packed or even in direct contact with each other. Consequently, this area is highly susceptible to transverse matrix cracking.

4. CONCLUSIONS

The manufacturing process of rotationally symmetric CFRP components, particularly during autoclave curing, can induce a significant FVF gradient across the laminate thickness. This gradient results from the thermal expansion of the mandrel, which generates tension in the circumferentially wound fibers and contact pressure at the mandrel-laminate interface. Under certain process parameter conditions, this tension is released through resin flow in the thickness direction. As a consequence, the cured laminate exhibits an FVF gradient, with a maximum in

FVF near the mandrel and a minimum in FVF approximately two-thirds away from it. A moving average analysis across the full laminate thickness revealed FVF spreads of 11.6 %pts. for the Hexcel 6376 specimens and 4.5 %pts. for the Teijin Q183 specimens.

The methodology developed in this study employed a simplified and scaled specimen geometry, representing a single-curved cylindrical section of a liquid hydrogen tank. A dedicated manufacturing rig was designed to enable faster and more cost-efficient specimen production while mimicking the automated fiber placement (AFP) process. The integration of Tekscan FlexiForce sensors at the mandrel-laminate interface provided valuable insights into contact pressure variations during the autoclave cycle, a phase typically difficult to observe due to the harsh environment and limited accessibility. The pressure measurements closely correlated with resin flow, offering a direct means of analyzing the underlying mechanisms governing resin flow in the thickness direction.

Finally this study explained how competing mechanisms are at play during mandrel curing: fiber hoop stress induced compaction stress, which is counteracted by viscous drag leading to percolation flow. By deconvoluting these principal effects it also points at the potential to match the resin rheokinetics, curing cycle and mandrel in future processes. Inhomogeneities introduced during manufacturing, such as FVF gradients, are often overlooked in the design phase. Given that prepreg systems are typically optimized for FVFs within ±1 %pt., the observed spreads are substantial. A key question that remains is whether the FVF gradient impacts the mechanical performance or permeability of the laminate. The findings from this study contribute to the broader effort of developing leak-tight and, therefore, safe storage solutions for liquid hydrogen, a crucial component in the transition toward sustainable aviation and the fight against climate change.

5. AUTHOR CONTRIBUTIONS

J.P.A. and P.S. conceived the investigation, carried out the experiments and enhanced the micrograph methodology to the given case. J.P.A. wrote the original manuscript. P.S. served as the daily supervisor. J.N. and C.B. provided the segmentation model and heatmap generation code. J.N. contributed to the editing of the section about the segmentation model and FVF heatmaps. B.A.V., C.D. and D.S. provided academic guidance and supervision.

6. ACKNOWLEDGMENT

The authors thank Elena Venutti for her hands-on support and companionship in manufacturing the specimens and for her expertise in optical microscopy. This work was part of the DLR-internal project HYTAZER. In addition, this work was funded by the German Federal Ministry of Economic Affairs and Climate Action (BMWK) under grant number 20M2113C (ZEIT – Zero Emission Industrial Technologies) and by the Investitions- und Förderbank Niedersachsen (NBank) under grant number ZW180159716 (HyStor – Hydrogen Storage).

7. REFERENCES

[1] IEA, "The Future of Hydrogen," IEA, Paris, 2019.

[2] J. Huete and P. Pilidis, "Parametric study on tank integration for hydrogen civil aviation propulsion," *International Journal of Hydrogen Energy* 46(74), pp. 37049-37062, 2021. DOI:

10.1016/j.ijhydene.2021.08.194

[3] Airbus Deutschland GmbH et al., "Liquid Hydrogen Fuelled Aircraft - System Analysis," 2003.

[4] A. Air, M. Shamsuddoha and G. Prusty, "A review of Type V composite pressure vessels and automated fibre placement based manufacturing," *Composites Part B: Engineering* 253, p. 110573, 2023. DOI: 10.1016/J.COMPOSITESB.2023.110573

[5] M. Azeem, H. H. Ya, M. A. Alam, M. Kumar, P. Stabla, M. Smolnicki, L. Gemi, R. Khan, T. Ahmed, Q. Ma, M. R. Sadique, A. A. Mokhtar and M. Mustapha, "Application of Filament Winding Technology in Composite Pressure Vessels and Challenges: A Review," *Journal of Energy Storage* 49, p. 103468, 2022. DOI: 10.1016/J.EST.2021.103468

[6] D. M. Grogan, "Damage and permeability in linerless composite cryogenic tanks," Galway, 2015.

[7] D. M. Grogan, S. B. Leen, C. O. Semprimoschnig and C. M. Ó Brádaigh, "Damage characterisation of cryogenically cycled carbon fibre/PEEK laminates," *Composites Part A: Applied Science and Manufacturing* 66, pp. 237-250, 2014. DOI: 10.1016/j.compositesa.2014.08.007

[8] A. Ahmed, B. Tavakol, R. Das, R. Joven, P. Roozbehjavan and B. Minaie, "Study of thermal expansion in carbon fiber-reinforced polymer composites," *SAMPE International Symposium Proceedings, Charleston, SC,* 2012.

[9] W. Alhaddad, M. He, Y. Halabi and K. Y. M. Almajhali, "Influence of Fiber Volume Fraction on the Predictability of UD FRP Ply Behavior: A Validated Micromechanical Virtual Testing Approach," *Materials* 17(19), p. 4736, 2024.

[10] H. Schürmann, "Wichtige Kenngrößen der Einzelschichten und des Laminats," in *Konstruieren mit Faser-Kunststoff-Verbunden*, Berlin, Heidelberg, Springer-Verlag, 2005.

[11] Deutsches Zentrum für Luft- und Raumfahrt e.V., "HyStor - Hydrogen Storage," 2023. [Online]. Available: https://www.dlr.de/de/zlp/forschung-transfer/projekte/projekte-aus-stade/projekt-archiv-stade/hystor.

[12] Hexcel Corporation, "Hexcel 6376 Data Sheet," 2025. [Online]. Available: https://www.hexcel.com/user_area/content_media/raw/HexPly_6376_eu_DataSheet.pdf.

[13] Teijin Carbon Europe GmbH, "Teijin Q183 Data Sheet," 2025. [Online]. Available: https://www.teijincarbon.com/fileadmin/user_upload/Datenbl%C3%A4tter/Thermosets/Product_Data_Sheet_TSG11en__Q183_series_.pdf.

[14] J. Kwik, "Entwicklung eines Materialmodells zur Vorhersage von Schäden an Faserhalbzeugen während automatisierter Ablegeprozesse," Deutsches Zentrum für Luft- und Raumfahrt e.V., Stade, 2019.

[15] METTLER TOLEDO, "Advanced Multi-Frequency TMDSC," 2025. [Online]. Available: https://www.mt.com/at/de/home/library/product-brochures/lab-analytical-instruments/stare_topem_datasheet.html.

[16] Tekscan, Inc., "FlexiForce HT201 Sensor," 2025. [Online]. Available: https://www.tekscan.com/products-solutions/force-sensors/flexiforce-ht201-sensor.

[17] J. Naumann, J. P. Appels, P. Sämann, T. de Wolff and C. Brauer, "Enhancing Composite Micrograph Analysis with Semantic Segmentation," in *Proceedings of SAMPE 2025*, Indianapolis, 2025.

[18] O. Ronneberger, P. Fischer and T. Brox, "U-Net: Convolutional Networks for Biomedical Image Segmentation," in *Medical Image Computing and Computer-Assisted Intervention - MICCAI 2015*, Munich, Germany, Springer, 2015, pp. 234-241. DOI: 10.1007/978-3-319-24574-4_28

[19] H. Darcy, Les fontaines publiques de la ville de Dijon: exposition et application des principes à suivre et des formules à employer dans les questions de distribution d'eau, Gent, Belgium: Victor Dalmont, 1856.